12th International Symposium on Turbulence and Shear Flow Phenomena (TSFP12)
Osaka, Japan (Online), July 19-22, 2022

DIRECT NUMERICAL SIMULATIONS OF OSCILLATORY BOUNDARY LAYERS OVER ROUGH WALLS

Umberto Ciri
Dept. of Mechanical Engineering
University of Puerto Rico at Mayagüez
PO Box 9000, Mayagüez, PR 00680, US
umberto.ciri@upr.edu

Sylvia Rodríguez-Abudo
Dept. of Engineering Sciences and Materials
University of Puerto Rico at Mayagüez
PO Box 9000, Mayagüez, PR 00680, US
rodriguez.abudo@upr.edu

Stefano Leonardi
Dept. of Mechanical Engineering
The University of Texas at Dallas
800 W Campbell Rd, Richardson, TX 75252 US
stefano.leonardi@utdallas.edu

ABSTRACT

Turbulent oscillatory flow over a rough bed is investigated with direct numerical simulations. Flow motion is induced by harmonic oscillation of the bed and the fluid is otherwise at rest, similarly to the classical Stokes boundary layer problem for the laminar flow over an oscillating flat plate. In the present case, the bed is rough and consists of two layers of fixed, identical spherical particles. In the turbulent flow, the oscillatory motion is propagated more rapidly from the bed to the bulk of the flow. At each distance from the bed, the time delay is reduced compared to the laminar linear trend and follows a curve which seems to depend primarily on the Reynolds number, rather than the particular bed configuration (rough or smooth). During the decelerating phase of the cycle, a log layer is observed in the velocity profiles, which is later suppressed in the acceleration phase. The Reynolds stresses resemble the canonical uni-directional boundary layer distribution in the deceleration phase and change sign as the flow reverses. Nevertheless, the production of turbulence kinetic energy does not achieve large negative values and remains positive. The phase of maximum turbulent kinetic energy production is anticipated compared to smooth beds, and depends on the rough bed morphology.

INTRODUCTION

Turbulent oscillatory boundary layers are a common hydrodynamic feature at the seabed of littoral zones. The oscillatory motion is generated by sea surface waves through gravity, and it affects the whole bed dynamics and morphology, from sediment erosion to transport and deposition patterns. Thus, the understanding of the oscillatory dynamics of a wall-bounded flow has both intellectual and practical consequences.

In the laminar regime, the oscillatory motion close to a solid wall is fairly well-known and can be described by the Stokes boundary layer. The Stokes boundary layer is a shear-driven flow generated by the harmonic oscillations of a flat plate respect to a fluid at rest in the far field. According to the classical solution (Batchelor, 1967), the governing parameters of the problem are the amplitude of the plate velocity oscillations U_0, and the characteristic length $\delta = \sqrt{2\nu/\omega}$, where ν is the fluid viscosity, and ω the frequency of the oscillations. The length δ is a measure of the distance from the plate up to which the effect of the oscillation is felt in the fluid domain (thus, from a reference frame on the oscillating plate, it represents the thickness of the boundary layer). Additionally, the laminar solution shows that the wall shear stress (also harmonic) has a phase lead of $\pi/4$ over the velocity oscillations.

More recently, various authors have investigated the oscillatory boundary layer over smooth walls, either numerically (Spalart and Baldwin, 1989; Akhavan et al., 1991b; Salon et al., 2007) or experimentally (Hino et al., 1983; Jensen et al., 1989; Akhavan et al., 1991a; Sarpkaya, 1993; Eckmann and Grotberg, 1991), for a wide range of flow conditions. Although in the experimental apparatus or numerical frameworks the oscillations are mostly imposed through an harmonic pressure gradient, the flow regime appears to still scale with the parameters identified by the shear-driven classic analysis, δ and U_0, and, in particular, with the Reynolds number $Re_\delta = U_0\delta/\nu$. Up to $Re_\delta \simeq 100$, the oscillatory boundary layer is laminar and follows the Stokes solution. As the Reynolds number is progressively increased, perturbations in the flow field appear and grow for some phases of the oscillation cycle. The boundary layer develops into two intermediate flow regimes (the 'disturbed laminar' and the 'intermittently turbulent' regime; Sarpkaya, 1993; Blondeaux & Vittori, 1994), before a fully developed turbulent regime is established. In the fully developed regime, $Re_\delta \gtrsim 750 - 1000$ (Hino et al., 1983; Jensen et al., 1989), turbulent fluctuations are present essentially throughout the whole period. The intensity of the fluctuations is larger during the deceleration interval (where perturbations starts to appear before extending to earlier and earlier phases while Re_δ is increased). The phase lead between the peak shear stress (no longer harmonic) and the maximum velocity is reduced compared to the laminar solution.

While the smooth wall provides a useful theoretical abstraction, in practice the Stokes layer will be bounded by a rough wall, in particular in coastal environments. Various studies have emphasized the importance for transition to turbu-

lence of even very small imperfections in otherwise "mirror-shine" smooth walls (Blondeaux & Vittori, 1994; Vittori and Verzicco, 1998; Costamagna et al., 2003; Verzicco and Vittori, 1996; Tuzi and Blondeaux, 2008). Other works have focused on large scale modulations of the bedform, ripples, which are often observed in various patterns as a result of sediment transport and deposition process by the oscillatory boundary layer (Grigoriadis et al., 2012; Penko et al., 2013; Rodríguez-Abudo and Foster, 2014; Scandura et al., 2000; Chang and Scotti, 2004; Önder and Yuan, 2019). On the other hand, Sleath (1987) and Jensen et al. (1989) have considered rough flat beds packed with sand, gravel or pebbles of various size, analogous to the classic configurations extensively analyzed in the context of steady boundary layers (Nikuradse, 1933). Sleath (1987) emphasized the role of vorticity 'bursts' or 'jets' associated with the wakes of the individual roughness elements, which separate and propagate from the wall to the outer layer when the flow reverses direction. The experiments of Jensen et al. (1989) at larger Re_δ suggested a similar scenario to steady rough-wall boundary layers, with the flow approaching a 'fully-rough' regime, where the main scaling parameter is the roughness size. In general, a complete understanding of rough-wall oscillating boundary layers is still lacking. In this work, we discuss results from direct numerical simulations of shear-driven oscillatory flow over a bed of spherical particles.

NUMERICAL METHODOLOGY

The non-dimensional continuity and Navier-Stokes equations are taken as the governing equations:

$$\frac{\partial U_i}{\partial x_i} = 0; \quad \frac{\partial U_i}{\partial t} + \frac{\partial U_i U_j}{\partial x_j} = -\frac{\partial P}{\partial x_i} + \frac{1}{Re_\delta}\frac{\partial U_i}{\partial x_j^2} \qquad (1)$$

where U_i is the velocity component in direction x_i and P is the pressure. The numerical method for solving the governing equations is described in Orlandi (2000). The substrate particles are treated with the immersed boundary method presented in detail in Orlandi and Leonardi (2006). Simulations are performed for an open channel with a bed of spherical particles on the lower wall (figure 1). The spheres are identical and regularly distributed into two superposed layers, with the bottom layer staggered by a radius. The lower boundary of the computational domain is tangent to the spheres of the upper layer, so that only the upper cap of the bottom spheres is inside the computational domain (see the inset in figure 1a).

This rough wall reproduces one of the configurations analyzed in Chan-Braun et al. (2011) and Mazzuoli and Uhlmann (2017) for a uni-directional pressure forcing at a Reynolds number based on the bulk velocity equal to $U_0 H/\nu = 2870$, where H is the height of the computational domain. This would correspond to a smooth-wall channel at $Re_\tau = u_\tau H/\nu = 180$, where u_τ is the friction velocity. In the present work, we have considered two values for the sphere diameter D, such that $H \approx 5.5D$ and $H \approx 10D$. The larger-particle case ($H = 5.5D$) reproduces the geometry in Chan-Braun et al. (2011), while the second case, for the small spheres ($H \approx 10D$), is obtained by halving the diameter of the spheres.

In the directions parallel to the bed, the computational domain is $6H$ (streamwise) and $3H$ (spanwise). For the case $H = 5.5D$, the mesh consists of $768 \times 384 \times 256$ uniformly distributed points in the streamwise, spanwise and bed-normal direction respectively. For the case $H = 10D$, the points have been doubled in the streamwise and spanwise direction ($1536 \times 768 \times 256$) to have sufficient resolution to model the particles. The resolution is consistent with the study of Chan-Braun et al. (2011).

As boundary conditions, periodicity is applied in the streamwise and spanwise directions. Free-slip is applied at the top of the domain. We consider the flow motion under an oscillatory shear-driven forcing, applied as a boundary condition with the immersed boundary method on the bed of spherical particles. The layers of sphere oscillate following the harmonic function in figure 1b, $U_0 \sin(\omega t)$. Four cases have been run, corresponding to a Reynolds number $Re_\delta = U_0\delta/\nu = 100$, 190, 765 and 1200, where δ is the depth of the Stokes layer ($\delta = \sqrt{2\nu/\omega}$). These last values are above (or at least approaching) the smooth-wall critical value for the fully-developed regime (Hino et al., 1983; Jensen et al., 1989).

RESULTS

Figure 2a summarizes the various cases analyzed in a 'Moody-diagram'-like chart, with the friction coefficient as a function of Re_δ. The bed drag varies in time throughout the cycle, and the friction coefficient C_f is defined with the maximum drag as $C_f = 2\tau_{\max}/\rho U_0^2$, where $\tau_{\max}$ is the maximum bed friction over the oscillation period and ρ the fluid density. The simulation results are compared with the analytical results for smooth-wall oscillatory flows in the laminar (Batchelor, 1967) and turbulent (Fredsøe, 1984) regimes.

It is apparent from figure 2a that the flow regime over the spherical bed with $H/D = 5.5$ scales with Re_δ similarly to the smooth wall case. At low Reynolds numbers, when the regime is laminar, the friction coefficient has an inverse dependence on Re_δ. The highest value of Reynolds number tested herein ($Re_\delta = 1200$) is approaching the fully turbulent regime. Simulations for the bed with small spherical particles ($H/D = 10$) have been performed for the two highest values only of $Re_\delta = 765, 1200$ to limit the computational cost. The trend in the transitional and turbulent regime is consistent with the case $H/D = 5.5$.

The bed friction as a function of time is shown in figure 2b, for the four Reynolds number cases. For the tests at low Re_δ, the shear waveform $\tau/\tau_{\max}$ resembles the laminar smooth wall case, $\cos(\omega t - \pi/4)$, but the maximum value is larger (fig. 2a) because the bed is rough. As the Reynolds number is increased, transition to the turbulent regime occurs and the friction coefficient increases compared to the laminar case. The shear stress further departs from the laminar behavior, as the waveform is no longer harmonic and the phase shift in the zero-crossing increases.

Turbulence over the rough bed induces further modifications in the temporal evolution of the flow, compared to the laminar case. Figure 3 shows the phase shift in the flow velocity with respect to the oscillatory forcing ($U \sin \omega t$), as a function of the distance from the bed. According to the Stokes' solution, the phase shift increases linearly (in magnitude) with the distance from the bed as the velocity is proportional to $\sin(\omega t - z/\delta)$. For the present simulations, the phase shift has been determined by first computing the time correlation between the sinusoidal forcing and the velocity signal at different distances from the bed. Then, the time shift τ corresponding to the maximum correlation has been taken to calculate the phase delay as $\varphi = \omega\tau$.

Figure 3 presents results for both the rough-bed configurations and a corresponding smooth wall simulation at the same Re_δ. Compared to the classical solution, the phase delay is reduced when the flow becomes turbulent. The decrease is

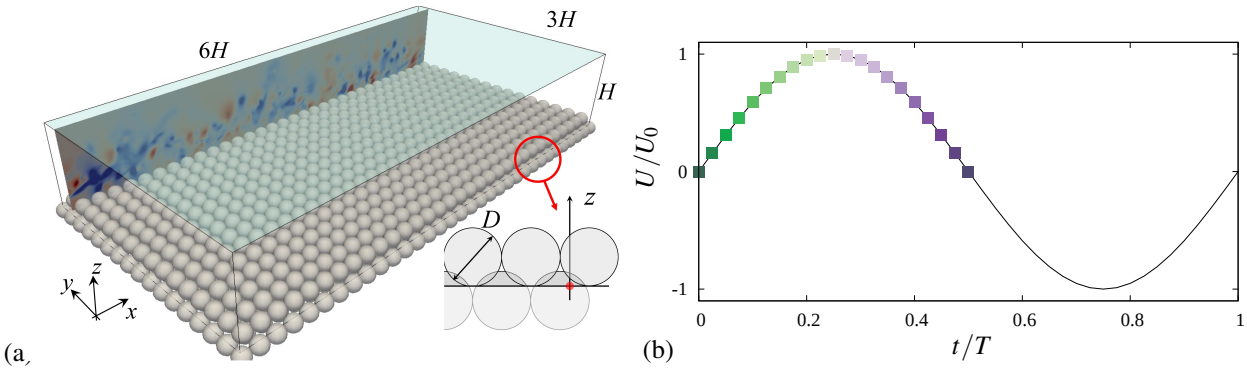

Figure 1. (a) Computational domain. (b) Oscillatory forcing and phase identifiers.

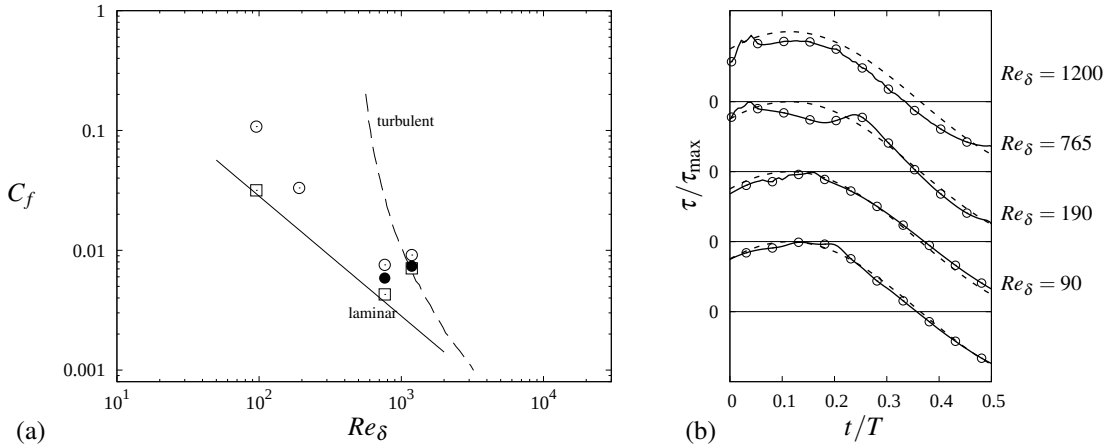

Figure 2. a) Friction coefficient C_f as a function of the Reynolds number. Symbols, present simulations: ○ spherical-particle bed, $H/D = 5.5$; • $H/D = 10$; □ smooth bed validation (Stokes boundary layer). Lines, theoretical trends for the laminar (Batchelor, 1967) and turbulent (Fredsøe, 1984) regimes (smooth bed). b) Wall friction variation over half-cycle for different Re_δ and $H/D = 5.5$ (lines are shifted vertically for the sake of clarity). Solid lines: present simulations for rough bed. Dashed line: Stokes solution, $\tau/\tau_{\max} = \cos(\omega t - \pi/4)$.

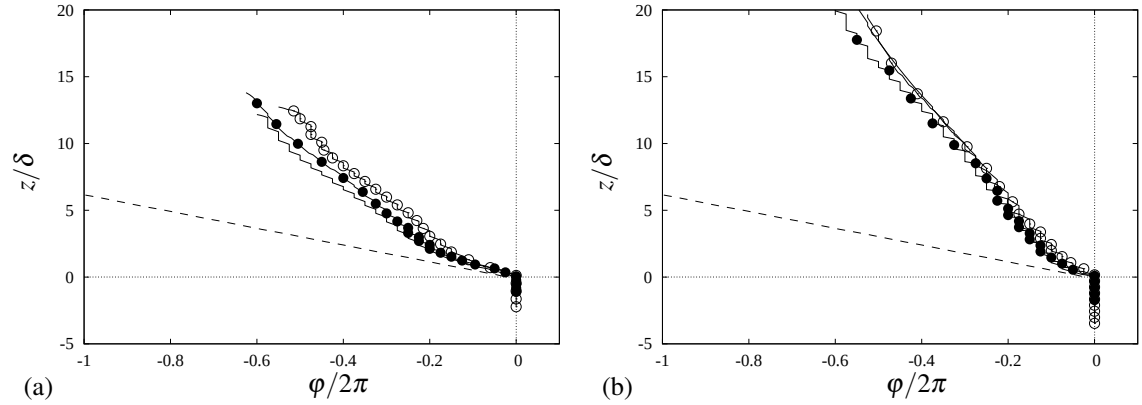

Figure 3. Velocity phase delay as a function of the distance from the bed for $Re_\delta = 765$ (a) and $Re_\delta = 1200$ (b). Symbols indicate present simulation over a rough bed: ○ $H/D = 5.5$; • $H/D = 10$. The solid line indicates present results for oscillating flow over a smooth bed. The dashed line shows the (laminar) theoretical trend from the Stokes' solution. The origin for z in the cases with the spherical-particle bed is taken at $0.2D$ below the crest plane.

significant already within a few Stokes depths δ from the wall ($z/\delta \lesssim 5$). This effect can be expected on the basis of a classic eddy-viscosity argument, with the macroscopic turbulent mixing enhancing the diffusion by molecular viscosity and propagating more rapidly the driving force from the wall to the bulk of the fluid. Consistently, the phase-shift reduction increases with the Reynolds number (as the flow approaches the fully turbulent regime) and it is observed at a shorter distance from the bed (figure 3a at $Re_\delta = 765$ vs. figure 3b at $Re_\delta = 1200$). It seems that this effect is controlled by the turbulent structures in the bulk of the flow, with little dependence on the shape or morphology of the bed. Both the cases with spherical particles ($H/D = 5.5$ and $H/D = 10$) and the smooth wall approximately collapse on a single curve with a slope which

depends on the Reynolds number. Possibly, at large values of Re_δ, in the fully-developed regime, a universal curve for the time delay may exist, where results collapse regardless of the bed morphology and Reynolds number.

Close to the bed, within approximately $z/\delta \lesssim 1$, the phase delay curve has the same slope as the laminar case (i.e. $\varphi/2\pi \approx -z/\delta$) regardless of the bed details and the Reynolds number. This region is the analogous of the viscous sub-layer in canonical uni-directional boundary layers. The flow remains laminar and the results collapse with the classical Stokes' theory.

Literature studies of smooth-wall oscillatory boundary layers report that intense turbulent activity is found in the deceleration phases, while fluctuations are damped in the acceleration phases (Jensen et al., 1989; Salon et al., 2007). Velocity profiles in wall units ($\overline{U}^+ = \overline{U}/u_\tau$) seem to confirm this scenario (figure 4). The friction velocity to scale the profiles corresponds the maximum friction over the cycle: $u_\tau = \sqrt{\tau_{\max}/\rho}$. The overline indicates an ensemble average in phase and in the streamwise and spanwise directions. The velocity profiles in figure 4 are evaluated in a reference frame moving with the oscillatory bed for the cases at $Re_\delta = 1200$ for half a cycle (the other half is symmetric in the present case). A logarithmic layer develops during the deceleration (purple lines), while it is not observed in the early phase of the cycle (acceleration, green lines). The logarithmic layer is observed also at $Re_\delta = 765$ (not shown here) in the decelerating phases. As expected, it occupies a thinner region of boundary layer, but this does suggest that turbulence starts developing already at $Re_\delta = 765$. The size of the spheres does not affect too much the time evolution of the profiles, as corresponding phases show similar features in terms of appearance of the logarithmic layer. The sphere diameter does change the downward shift of the profiles compared to the canonical law of the wall. The downward shift (i.e., the roughness function, ΔU) is related to the wall drag, and, consistently with figure 2a, it decreases for the case $H/D = 10$ (small spheres, and smaller drag).

Turbulence generation near the wall in the early deceleration phases results in large values of the Reynolds shear stress $\overline{uw}$. Figure 5 shows Reynolds stress profiles for the large sphere case ($H/D = 5.5$, panel a) and the small sphere case ($H/D = 10$, b). During the deceleration, the profiles resemble the typical uni-directional boundary layer case, with a (negative) near wall peak and an approximately linear decay in the outer layer, which depends on the total shear. The value of the near wall peak is approximately the same for both values of the particle diameter D and is approached at about the same phase of the cycle. Coherent structures generated during the deceleration phase propagate from the wall to the outer layer in the next phases of the cycle. Even if turbulence is damped in the acceleration phase, the Reynolds stress remains relatively large and changes sign as the flow reverses, which may potentially lead to negative turbulent kinetic energy (TKE) production. The turbulent kinetic energy production ($\mathscr{P} = -\overline{uw}\,\mathrm{d}\overline{U}/\mathrm{d}z$) is plotted in figure 6 for both values of D. The TKE production for a canonical unidirectional flow is also shown as reference. The peak value of TKE production appears reduced compared to the uni-directional flow because results in figure 6 are normalized with the maximum friction velocity ($\mathscr{P}^+ = \mathscr{P}\nu/u_\tau^4$, with $u_\tau = \sqrt{\tau_{\max}/\rho}$) which does not occur at the same phase as the maximum in the production. The maximum in friction (i.e., maximum in shear) occurs earlier in the cycle, towards the end of the acceleration phase (see figure 2b). Instead, turbulence production is large and peaks during the deceleration phases, when, consistently, a logarithmic layer is also established in the velocity profile. For the case with the large particles ($H/D = 5.5$), the peak in the production appears shifted at larger distance from the wall. However, this may be due to some uncertainty in the determination of the virtual origin for z, which herein is taken at $0.2D$ below the crest of the sphere following Chan-Braun et al. (2011). Negative values of production $\mathscr{P}$ are observed when the velocity changes sign, although the magnitude is very small. The production depends on both the Reynolds stress $\overline{uw}$ and the shear $\mathrm{d}\overline{U}/\mathrm{d}z$. As the forcing changes sign, the Reynolds stresses are large (and with opposite sign) in the outer layer where the velocity gradient is small. This is also the case for oscillatory flows over smooth beds (Salon et al., 2007). However, it is not straightforward to generalize this situation for other flow regimes or rough beds, since the sign of the production will ultimately depend on the interplay between the oscillatory forcing and time-scales associated with the rough bed. For example, ejections of coherent structures or shedding from the bed crests as the flow reverses direction may affect and change the sign of TKE production.

Figure 7 shows the evolution in time, throughout half the cycle, of the peak of TKE production $\mathscr{P}_{\max}$. The peak is normalized both with the maximum friction velocity (panel a; normalization as in figure 6) and with the instantaneous friction velocity (panel b), which depends on the local shear, $\tilde{u}_\tau = \sqrt{\tau(t)/\rho}$. Figure 7a shows that the maximum value of $\mathscr{P}_{\max}$ across the cycle is not attained at the same phase for the rough beds and the smooth wall. Instead, a large phase lead compared to the smooth wall reference is observed for the bed made of large spherical particles ($D/H = 5.5$). The phase lead is still present although somewhat mitigated for the case ($D/H = 10$). The phase shift in $\mathscr{P}$ (which can also be noted in figure 6) should be attributed to time evolution of the shear, rather than the Reynolds shear stresses $\overline{uw}$. From figure 5, it appears that $\overline{uw}$ are relatively well synchronized for both values D. The shear $\mathrm{d}\overline{U}/\mathrm{d}z$ seems to be more sensitive to particular configuration of the bed and causes the phase shift.

In figure 7b, the peak of TKE production is shown with the normalization by the instantaneous friction velocity. Since the shear vanishes during the cycle (figure 2b), the curve is singular. The zero-crossing of the wall shear stress is anticipated compared to the laminar case (which has a phase lead of $\pi/4$, corresponding to a zero crossing at $t = 3/8T = 0.375T$). Figure 7b confirms the increase in the phase lead for the rough bed cases, as the curve blows-up shortly after $t/T = 0.3$. This behavior is opposite to that of the turbulent oscillatory flow over a smooth wall, where the phase lead is reduced compared to the laminar solution, as it can be observed from the dashed line in figure 7 and literature results (Jensen et al., 1989).

CONCLUSIONS

Numerical simulations of turbulent oscillatory flow over a bed made of spherical particles have been performed. We have considered a shear-driven flow, where the bed moves according to an harmonic function and the fluid is otherwise at rest. The bed consists of two superposed layers of fixed, identical spherical particles. We have considered two different values of the particle diameter to investigate the dependence of the flow on the sphere size. Simulations have been performed for a range of Reynolds number, spanning from the laminar regime and approaching fully-developed turbulence.

Results show that the temporal evolution of the flow over the rough bed is modified compared to classical Stokes' solution for laminar boundary layers. In particular, the phase

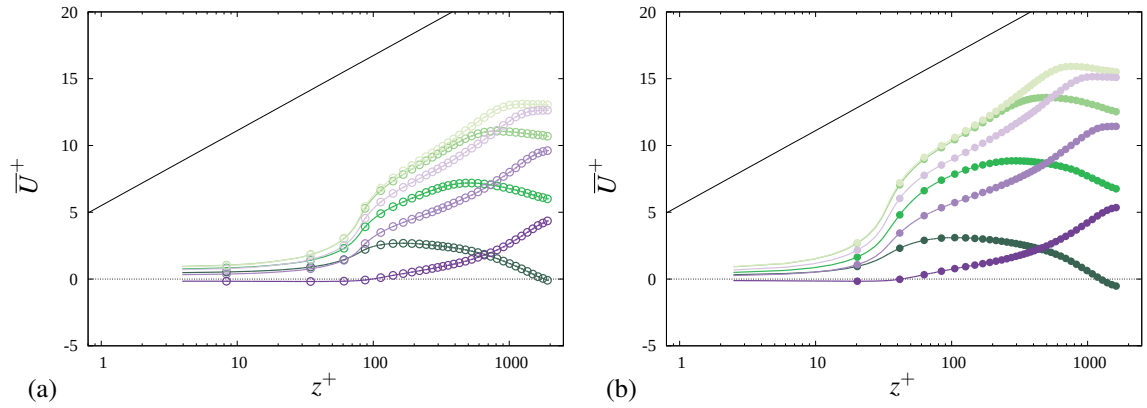

Figure 4. Mean velocity profile in wall units at different phases and law of the wall (solid line): $(1/\kappa)\log y^+ + B$, with $\kappa = 0.41$ and $B = 5.5$; (a) $H/D = 5.5$ large sphere case; (b) $H/D = 10$ small sphere case. Following Chan-Braun et al. (2011), the virtual origin of the profile is taken $0.2D$ below the crest of the spheres.

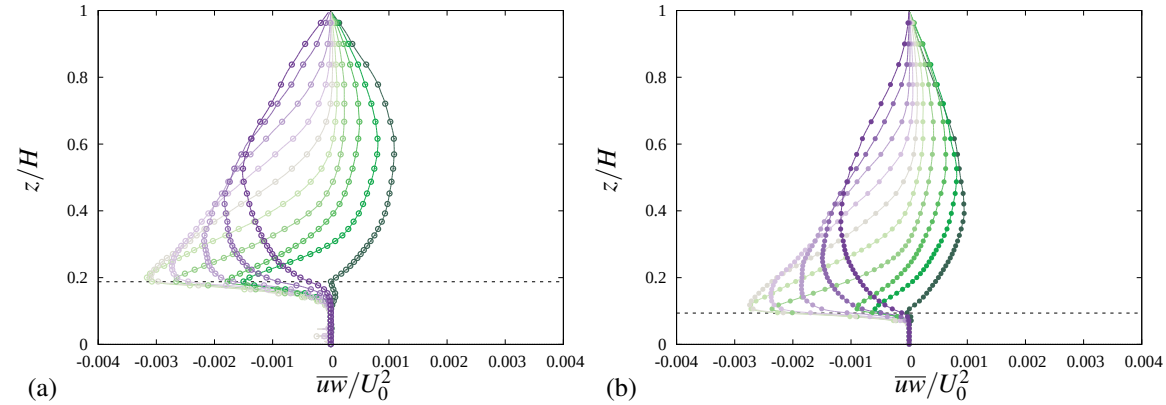

Figure 5. Reynolds shear stress $\overline{uw}$ profile at different phases of the oscillation: (a) $H/D = 5.5$ large sphere case; (b) $H/D = 10$ small sphere case. The horizontal dashed line indicates the crest plane. Colors indicate the phase as in figure 1b.

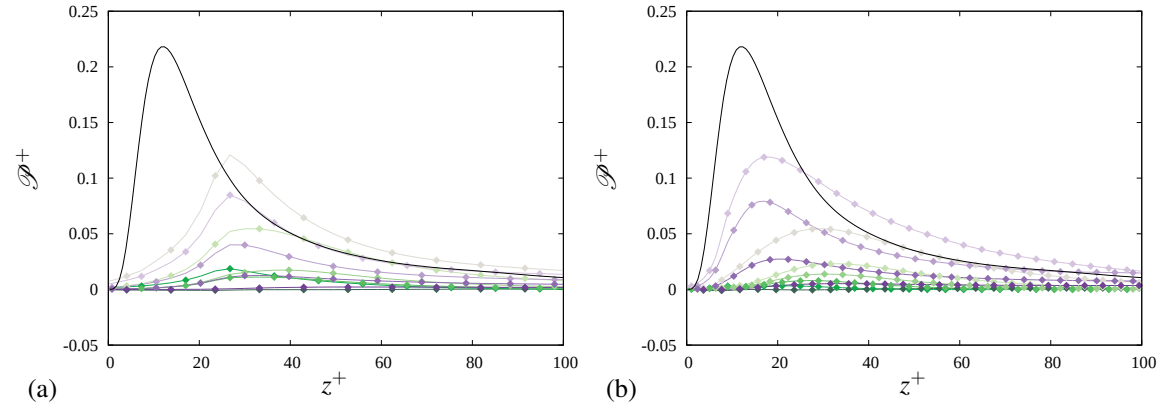

Figure 6. Turbulent kinetic energy production $\mathscr{P}$: (a) $H/D = 5.5$, large sphere case; (b) $H/D = 10$, small sphere case. The solid black line shows the production for a uni-directional turbulent boundary layer. Colors indicate the phase as in figure 1b for the oscillatory flow cases.

shift in the velocity at various distances from the bed is reduced compared to the laminar case, which predicts a linear increase (in magnitude) with the distance from the bed. The phase shift reduction seems predominantly dependent on the Reynolds number rather than the bed morphology, which suggests that a unique curve may exists for large enough values of the Reynolds number Re_δ. The bed drag also has a different phase shift compared to the laminar solution. In this case, as the flow becomes turbulent, the drag wave form is no longer harmonic and the zero-crossing occurs earlier in the cycle for the rough beds. An opposite behavior, with a delay in the zero crossing, is observed for turbulent oscillatory flows over smooth beds.

Strong turbulence activity is observed during the deceleration phases of the cycle, with the presence of a logarithmic layer in the velocity profile. During the acceleration, the logarithmic region is suppressed and the value of the Reynolds shear stress also decreases. However, the Reynolds stress re-

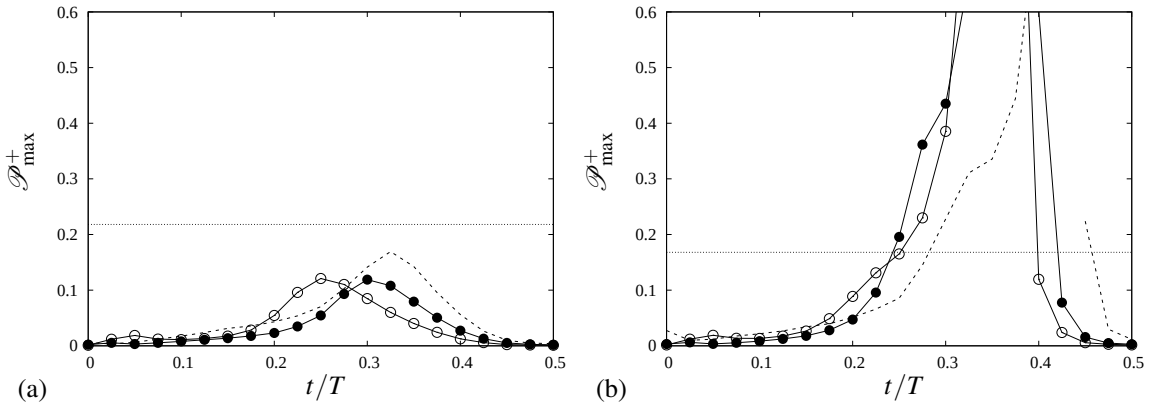

Figure 7. Evolution in time of the maximum of turbulent kinetic energy production $\mathscr{P}_{\max}$ normalized in wall units with the maximum friction velocity (a) and the instantaneous friction velocity (b): ∘ spherical-particle bed, $H/D = 5.5$; • $H/D = 10$; – – – – smooth wall. The horizontal line indicates the value for a unidirectional boundary layer over a smooth wall.

mains different than zero throughout the cycle and changes sign (compared to the canonical case in wall-bounded turbulence) as the flow reverses direction. Nevertheless, the turbulent kinetic energy production appears to remain positive (or just slightly negative) because the velocity gradient is very small during these phases. While this happens similarly for both rough bed configurations, the time evolution of the turbulent kinetic energy is not the same in the two cases. This is because production depends on both the time-scales of the oscillatory forcing and the overlying turbulent flow. Therefore, it may be possible to observe enhanced regions of negative TKE production for different bed configurations or flow regimes.

REFERENCES

Akhavan, R., Kamm, R. D. and Shapiro, A. H. 1991a An investigation of transition to turbulence in bounded oscillatory Stokes flows. Part 1. *J. Fluid Mech.* **225**, 395–422.

Akhavan, R., Kamm, R. D. and Shapiro, A. H. 1991b An investigation of transition to turbulence in bounded oscillatory Stokes flows. Part 2. *J. Fluid Mech.* **225**, 423–444.

Batchelor, G. K. 1967 *An Introduction to Fluid Dynamics*, Cambridge University Press.

Blondeaux, P. and Vittori, G. 1994 Wall imperfections as a triggering mechanism for Stokes-layer transition. *J. Fluid Mech.* **264**, 107–135.

Chang, Y. S. and Scotti, A. 2004 Modeling unsteady turbulent flows over ripples: Reynolds-averaged Navier-Stokes equations (RANS) versus large-eddy simulation (LES). *J. Geophys. Res.* **100**, C09012.

Chan-Braun, C., García-Villalba, M. and Uhlmann, M. 2011 Force and torque acting on particles in a transitionally rough open-channel flow. *J. Fluid Mech.* **684**, 441–474.

Costamagna, P., Vittori, G. and Blondeaux, P. 2003 Coherent structures in oscillatory boundary layers. *J. Fluid Mech.* **474**, 1–33.

Fredsøe, J. 1984 Turbulent boundary layer in wave-current motion. *J. Hyd. Engng. ASCE* **110**, 1103–1120.

Eckmann, D. M. and Grotberg, J. B. 1991 Experiments on transition to turbulence in an oscillatory pipe flow. *J. Fluid Mech.* **222**, 329–350.

Grigoriadis, D. G. E., Dimas, A. A. and Balaras, E. 2012 Large-eddy simulation of wave turbulent boundary layer over ripple bed. *Coastal Engineering* **60**, 174–189.

Hino, M., Kashiwayanagi, M., Nakayama, A. and Hara. T. 1983 Experiments on the turbulence statistics and structure of a reciprocating oscillatory flow. *J. Fluid Mech.* **131**, 363–400.

Jensen, B. L., Sumer, B. M. and Fredsøe, J. 1989 Turbulent oscillatory boundary layers at high Reynolds numbers. *J. Fluid Mech.* **206**, 265–297.

Mazzuoli, M. and Uhlmann, M. 2017 Direct numerical simulation of open-channel flow over a fully rough wall at moderate relative submergence. *J. Fluid Mech.* **824**, 722–765.

Nikuradse, J. 1933 Stromungsgesetze in rauhen Rohren. *Forschungshelft* **361** (Engl. transl. *NACA TM* 1292).

Önder, A. and Yuan, J. 2019 Turbulent dynamics of sinusoidal oscillatory flow over a wavy bottom. *J. Fluid Mech.* **858**, 264–314.

Orlandi, P. 2000 *Fluid Flow Phenomena: a numerical toolkit*. Kluwer Academic Publishers.

Orlandi, P. and Leonardi, S. 2006 DNS of turbulent channel flows with two- and three-dimensional roughness. *J. Turbul.* **7**, N73

Penko, A. M., Calantoni, J., Rodriguez-Abudo, S., Foster, D. L. and Slinn, D. N. 2013 Three-dimensional mixture simulations of flow over dynamic rippled beds. *J. Geophys. Res.* **118**, 1543–1555.

Rodríguez-Abudo, S. and Foster, D. L. 2014 Unsteady partitioning and momentum transfer in the wave bottom boundary layer over movable rippled beds. *J. Geophys. Res.: Oceans* **119**, 8530–8551.

Salon, S., Armenio, V. and Crise, A. 2007 A numerical investigation of the Stokes boundary layer in the turbulent regime. *J. Fluid Mech.* **570**, 253–296.

Sarpkaya, T. 1993 Coherent structures in oscillatory boundary layers. *J. Fluid Mech.* **253**, 105–140.

Scandura, P., Vittori, G. and Blondeaux, P. 2000 Three-dimensional oscillatory flow over steep ripples. *J. Fluid Mech.* **412**, 355–378.

Sleath, J. F. A. 1987 Turbulent oscillatory flow over rough beds. *J. Fluid Mech.* **182**, 369–409.

Spalart, P. R. and Baldwin, B. S. 1989 Direct Simulation of a Turbulent Oscillating Boundary Layer. In *Turbulent Shear Flows 6*, pp. 417–440. Springer-Verlag.

Tuzi, R. and Blondeaux, P. 2008 Intermittent turbulence in a pulsating pipe flow. *J. Fluid Mech.* **599**, 51–79.

Verzicco, R. and Vittori, G. 1996 Direct simulation of transition in Stokes boundary layers. *Phys. Fluids* **8**, 1341–1343.

Vittori, G. and Verzicco, R. 1998 Direct simulation of transition in an oscillatory boundary layer. *J. Fluid Mech.* **371**, 207–232.